



Comparison of ultrasonic and other atomization methods in metal powder production

B. Bałasz^a, M. Bielecki^{b,*}, W. Gulbiński^a, Ł. Słoboda^{b,c}

^a Koszalin University of Technology, ul. Śniadeckich 2, 75-453 Koszalin, Poland

^b 3D Lab Ltd., ul. Farbiarska 63B, 02-862 Warszawa, Poland

^c AGH University of Science and Technology, Al. Mickiewicza 30, 30-059 Kraków, Poland

* Corresponding e-mail address: marcin.bielecki@3d-lab.pl

ORCID identifier:  <https://orcid.org/0000-0003-2397-7722> (M.B.)

ABSTRACT

Purpose: Additive manufacturing (AM) research needs new alloys to grow and offer new functionalities. This paper presents a novel powder production method by means of ultrasonic atomisation (UA). Powders for AM can be obtained from gas atomisation (GA) and a comparative study of UA- vs GA-made powders were carried out. To UA explain the pros & cons more clearly, a summary of the processes was added, along with the analysis of the droplet formation physics.

Design/methodology/approach: Ultrasonic atomization (UA) with melting raw material by an electric arc. Characterisation of the powders: particle size distribution (PSD), density, and flowability were carried out. Other parameters, such as microstructure, deviation in the chemical composition and powder surface morphology, were also investigated.

Findings: The results showed that the UA powder has a finer average particle size with a narrower statistical distribution of particles than those made by the GA method. Because the UA powder has a higher sphericity and lower porosity, Generally, UA offers better-quality powders in terms of properties such as higher tap density, better flowability and low oxygen content.

Research limitations/implications: As an example of semi-industrial scale application of the UA system, the Ti6Al4V and TiAl powders were produced after remelting the wire. The UA system is commercially available for processing any metallic material.

Practical implications: The test campaign results showed that the Ti6Al4V powder produced by the ultrasonic atomisation has a similar or better quality as those available from large-scale gas atomisation plants.

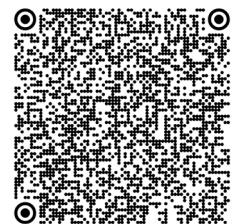
Originality/value: The new method of UA powder production was analysed in terms of key powder parameters. The properties of the titanium-based powder produced this way were analysed with a view to future applications.

Keywords: Powder metallurgy, Metallic alloy, Atomization, Additive manufacturing, Titanium

Reference to this paper should be given in the following way:

B. Bałasz, M. Bielecki, W. Gulbiński, Ł. Słoboda, Comparison of ultrasonic and other atomization methods in metal powder production, Journal of Achievements in Materials and Manufacturing Engineering 116/1 (2023) 11-24. DOI: <https://doi.org/10.5604/01.3001.0016.3393>

MANUFACTURING AND PROCESSING



1. Introduction

Metal powders are used in everyday applications. Powder metallurgy methods are commonly applied in advanced coatings and advanced materials and processes like 3D printing. Price is still an issue, and relatively popular materials like Titanium Grades 2 and 5 are still expensive, with average market prices at €210 per kilogram according to the 2020 data.

Typically, the required powders are in size range of 15-60 µm for additive manufacturing and 50-100 µm for coatings. The most common production methods for fine powders are gas atomisation (GA) and plasma (PA) atomisation; both can meet the demands of highly spherical powders in high volumes. A comprehensive review of the production methods of titanium-based powders, including chemical methods, can be found in [1-3]. Considering the applications for the AM market, spherical Ti alloy powders with a low oxygen content and good flowability are in high demand. Unfortunately, high-quality spherical Ti alloy powders are costly and in low supply. This hinders the titanium development for applications employing AM and other advanced manufacturing processes. Therefore, the industry is strongly urged to develop new processes for producing low-cost Ti-based powders, which could meet all physical and chemical requirements. The paper also looks at the factors that significantly impact the powder cost, like consumables and energy demand.

One of the alternatives to powder production is a process known as Ultrasonic Atomization (UA). By using Ultrasonic Vibrations on a liquid material, it is possible to induce Rayleigh wave instability, which causes the effect of uncontrolled generation of small metal droplets, which become the desired powder in the cooling process. The molten metal ensures that premium quality powders are obtained at a lower cost than with other popular methods such as Gas Atomization (GA), Plasma Atomization (PA) or Plasma Rotating Electrode Process (PREP). Note that GA technology is present in many versions on the market, although the most comparable Electrode Induction Gas Atomization (EIGA) is commonly used for titanium alloys, which are discussed in the article [4].

Producing powder in small amounts in laboratory conditions as an additional pre-processing step for a small-scale additive manufacturing facility is a new trend in the market. The UA approach of forming droplets, followed by drying them to powder, is a well-known process in the pharmaceutical industry. It has been used for decades to atomise liquids on nebulisers. The technology discussed here is based on a similar principle but with molten metal. The equipment is fitted with a melting system capable of

turning titanium alloys into liquid at temperatures above 1660°C.

The UA technology allows us to produce spherical particles with diameters suitable for 3D printing technologies such as LPBF / SLM / BMLM / DMLS / DED / DM / LMD. One of the properties of such powders that is critical to quality (CTQ) is their residual porosity – especially as regards high-end materials like titanium alloys applied by default in heavy-duty applications. According to research [5], porosity is anticipated to affect the fatigue properties of final parts after 3D printing and sintering, which may require an expensive HIP process to reduce their porosity. To assure a low porosity of AM parts, the powder should be free of gas bubbles (i.e., its true density is required to be as close as possible to the theoretical one). It should have good flowability to allow a uniform distribution of particles in the bed. The sintering process requires optimisation as well, as proven in [6].

A compact UA system allows high-quality metal powders for any new alloy composition to be quickly produced in less than one day. The UA unit may be compared to a gas atomisation system, which, even at its most inexpensive configuration, can cost well over €1 million, without including the additional costs of infrastructure. Compared to the currently available atomisation technologies, the ATO system has a considerably lower media consumption as the atomisation takes place at a pressure of ~1.1 bar, while e.g. the gas atomisation is run at a pressure of 15-60 bar, in much larger volumes, and the droplets have a very high speed during formation. As a result, not only is the cost-effective UA process easy and rapid, but it is also attractive from a business point of view for virtually any high-end or customised alloy produced in a small or medium quantity.

This paper summarises atomisation tests on a standard titanium alloy Ti6Al4V. However, the same system has been tested [7] in the production of high alloy steel and nickel-based alloys, e.g., Inconel grades. In addition, custom versions of the system meet customer expectations for cost-effective powder production of silver, gold, and platinum as well as other rare and expensive alloys. The unique features of the ATO system are protected by international patents [8-10].

2. Description of the ultrasonic atomisation process

The ATO system works, in general, by means of an ultrasonic horn (sonotrode), which transfers mechanical energy obtained from the piezoelectric transducer to the

molten metal and turns it into fine droplets. A process like this is neither ultrasonic assisted gas atomisation nor ultrasonic standing wave atomisation, which are described in [11]. The ATO system integrates the raw metal melting by an electric arc with the atomisation by ultrasound vibrations in the molten metal pool. Other research teams have validated a similar concept [12-14].

The ultrasonic atomisation as tested here is executed in the following steps – see the movie provided by 3D Lab [15]:

1. The raw material in the form of a wire or a rod is continuously supplied to the atomisation chamber. The material is placed on the sonotrode, where the atomisation takes place.
2. An electric arc is formed between a non-consumable electrode and the sonotrode due to the high voltage generated by a DC generator.
3. The next step involves melting the raw material on the upper (hot) end of the sonotrode to form a molten metal pool.
4. The ultrasonic vibrations are transferred through the sonotrode from its cold end, where the ultrasonic transducer is connected, towards the hot end and eventually to the molten metal pool. The capillary waves are formed on its surface. Once the amplitude of the vibrations reaches the critical threshold, the capillary waves become unstable and form droplets. Their diameter is inversely proportional to the ultrasound frequency, although the surface tension and the molten metal density also play an important role.
5. The droplets are ejected in the stream of the cooled inert gas and directed with the flow. They stay in a liquid state near the electric arc for a short period of time until the surface tension shapes them to almost perfect spheres. Furthermore, the droplets cool down by heat transfer with the cold inert gas, then solidify in a fraction of a second, and with the aid of aerodynamic forces, are conveyed to the atomisation chamber outlet.
6. The stream of warm inert gas and powder is separated in a cyclone; then the powder is collected below the cyclone in a sealed container. The gas from the cyclone is filtered out of the dust (particles of a few microns), cooled, and recirculated back to the beginning of the cycle.

It is anticipated that in the foreseeable future pellets from scrapped and milled AM print-outs, as proposed in [16], could also be used as a raw material here.

To efficiently carry out the above actions, the machinery consists of several sub-systems which work with each other:

- raw material delivery system,
- melting system, which generates the electric arc that melts the input material,
- ultrasonic sub-system consisting of a sonotrode, waveguide and vibration generator to transfer the vibrations to the molten metal pool and eject the droplets of liquid metal,
- cooling gas sub-system with the atomisation chamber where droplets are formed and then cooled down to powder,
- gas-powder separation sub-system to collect powder and regenerate the gas.

2.1. Raw material melting sub-system

The main problem to be resolved for a successful UA of metals is to integrate the melting system with the ultrasonic vibration system. This is because the alloys for additive manufacturing need to be fully melted from an ambient 20°C to the optimal atomisation temperature, preferably about 1.3-1.5 times the material melting temperature (absolute). In the case of the Ti6Al4V alloy with the liquidus temperature at 1660°C, the optimal atomisation temperature is within the range of 2200-2600°C, although the heater setup allows for a higher heat rate when needed, e.g. when melting refractory metals. This higher temperature lowers the surface tension and viscosity of the molten metal to be atomised; this increases the atomisation output and reduces the size of droplets at a relatively low amplitude of the capillary waves. Further increases in the temperature during atomisation could cause evaporation losses of the most volatile elements in the atomisation chamber – for instance, aluminium, which has a boiling point at 2470°C. Optimally, the atomisation and the melting processes should take place in the same area. Previous setups melted the raw material (e.g., by induction heating like in [17]) significantly above the sonotrode, and then the liquid material drained down. Unfortunately, such an approach tends to splash the molten metal, eventually ending up with frequently interrupted atomisation and a poor-quality powder. So, the novel integrated heating for the UA system was engineered to combine melting and atomisation action on the sonotrode.

It means that at least two sub-systems need to be sized and adequately efficient to carry out two actions at the same time:

- Continuously supply heat to the raw material in order to increase its temperature (e.g., from ambient) to 1.3-1.5 times its melting temperature (incl. latent heat of recrystallisation and fusion), i.e. to fulfil the enthalpy demand
- Keep the above optimal temperature in the molten metal pool on the cooled sonotrode inside the cooled atomisation chamber.

The entire atomisation process takes place in an inert gas atmosphere, while the electric arc is started in the inert gas as well. Figure 1 shows the configuration of the heating device (torch) with the sonotrode and the raw material supply.

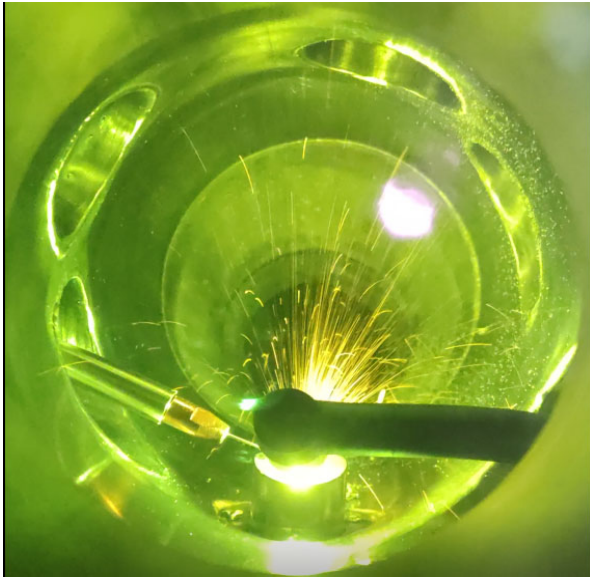


Fig. 1. Melting of a wire (at left) by an electric arc (centre – right) and the ejection of droplets from the sonotrode (at the bottom)

2.2. Ultrasonic sub-system and droplet ejection

Due to the strict physical relationship of ultrasonic vibrations, the obtained powder has a limited particle size distribution, which is strongly reliant on the chosen ultrasound frequency. For example, the powder batches made at a frequency of 35 kHz reach the average size of 62 μm for Ti6Al4V and 52 μm for Ti25Al12Nb alloys. Because a calibrated ultrasonic system and optimal electric arc heating are used, which creates a relatively uniform thermal flux towards the molten metal pool, a significant share of the powder has a diameter close to the desirable one. This physics-based phenomenon allows us to target the powder size and produce a batch with much a higher utilisation (conversion rate) than that of typical gas or plasma atomisation – see Figure 2, where the data marked with black triangles are based on [18], the data marked with black dots are based on [19]. The data marked with blue dots are based on [20].

Lang proposed a model to estimate the diameter D_{32} of the droplets (the so-called mean Sauter diameter) for a deep pool of water in 1964 [21]. It was subsequently extended in

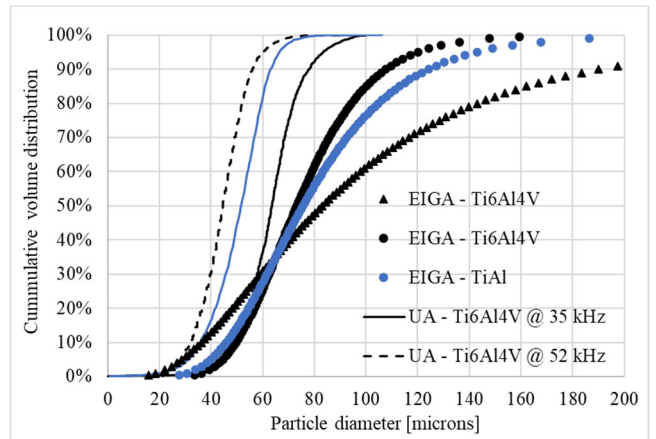


Fig. 2. Cumulative distribution of typical output from gas (EIGA) and ultrasonic (UA) atomisation for titanium alloys (before classification)

many research studies (e.g. [22, 23]) onto other more viscous liquids such as glycerine or hydrocarbons. Other research [24,25] focused on visualisation of the droplet formation at specific conditions. As proven by the tests on the ATO system, as well as found in the literature on low-melting metals (e.g., in [26] tested on Pb-Bi-Sn alloy and in [17] tested on aluminium alloys), the formula below, based on Lang's model is also valid for molten metals:

$$D_{32} = 0.34 * \lambda * f(We, Oh, In) \quad (1)$$

where λ is the length of the capillary wave on the liquid surface, and an empirical function $f(We, Oh, In)$ has dimensionless input variables of Weber's (We), Ohensorge's (Oh), Intensity (In) numbers. The term $f(We, Oh, In)$, unless assumed to be equal to 1.0 for simplicity, is the most important for the conditions of very aggressive ejection of droplets in more viscous liquids, i.e., at a high amplitude of ultrasonic vibrations just above the melting point, because the likelihood of forming the largest droplets in the population is mitigated with the aid of cavitation or just after ejection with the aid of aerodynamic forces. In such a case, instead of single large droplets, a group of smaller ones leave the atomisation zone. This eventually reduces the median and D_{32} of the entire powder population. In the most common version of the process on molten metal with a moderate production rate of the powder, this term can be neglected, hence the assumed $f(We, Oh, In) = 1.0$. The length of the capillary wave λ can be calculated from the equation:

$$\lambda = \sqrt[3]{\frac{8 * \pi * \sigma}{\rho_L * f^2} * \tanh\left(\frac{2 * \pi * h}{\lambda}\right)} \quad (2)$$

where: σ and ρ_L are respectively the surface tension and density of molten metal at a given temperature, f is the

ultrasonic frequency of the waves generated by the sonotrode, h is the depth of the liquid pool. The term $\tanh(\dots)$ in formula (2) represents a correction due to the shortening of the capillary waves in a shallow pool. A visualisation of the droplet formation is pictured in Figure 3. The process can be simulated in the CFD software with the aid of a VOF multiphase approach. e.g., as described in [25,27]. It shows that the capillary waves become unstable at the appropriately high amplitude, and some reject pieces of molten metal. As such, the ejection takes place in the hot gas (>3000 K), with the temperature determined by the electric arc; these pieces stay for a fraction of a second in liquid form so that the surface tension rounds them off to spheres, which then subsequently cool down and crystallise as powder.

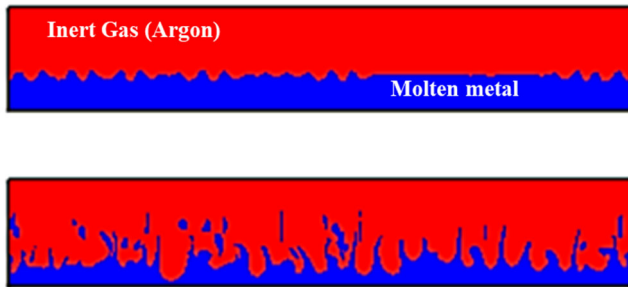


Fig. 3. Simulation of capillary waves in a shallow pool: top – low vibrations with stable waves, bottom – high vibration with unstable waves and droplet ejection

The above formulas provide a reasonable estimation of the average droplet diameters because the experimental statistical distributions of the powder batches tested show that the average powder diameter is almost equal to the D_{32} value. Moreover, one should take into account that the results of these formulas apply to droplets in a liquid state; hence in the case of metal powder, their diameters need to be further scaled down because of thermal contraction when cooled down to the ambient temperature. To avoid miscommunication, we present all the values of powder diameters in this paper after such scaling to a cold state (at 20°C) in order to be able to compare them to measurements on samples directly.

To estimate the powder diameter, the surface tension and density of the molten alloy at the pool temperature are needed. Unfortunately, the availability of material data can be challenging, as methods for measuring or estimating the surface tensions for metals are not very accurate. Typically, they have an error in the range of +/- 10%. These variations can be related to the measurement method as deliberated in [28, 29, 30], albeit from a practical point of view, it is usually

a secondary effect of alloying or contamination. Moreover, the temperature in the pool is easy to control (e.g., by adjusting the current in the electric arc), but difficult to measure, as thermal imaging cameras measure inaccurately in the presence of strong UV light from the electric arc and the ejected droplets, which partly overshadows the view on the pool. Usually, for a preliminary assessment of the most likely UA performance, the formulas (1) and (2) are simplified to:

$$D_{32} = 0.34 * \sqrt[3]{\frac{8 * \pi * \sigma(T)}{\rho_L(T) * f * \pi * q^2}} \quad (3)$$

Considering the analytical models as in (1) and (2) with empirical correction factors specific to the ATO system, one can estimate the average powder size for any alloy composition. The sensitivity study of the analytical model shows (summary in Fig. 4) that two main variables affect the powder diameter:

- the ultrasonic frequency, which, if doubled, would reduce the powder size by ~40%,
- the atomisation temperature as influencing the material properties of the molten metal (its surface tension and density).

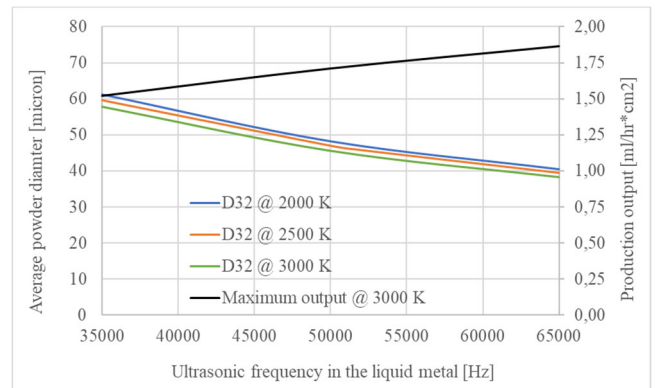


Fig. 4. Average powder diameter and the maximum possible production rate for the Ti4Al6V alloy as a function of ultrasonic frequency and atomisation temperature

As the first factor is the easiest to be applied for system performance optimisation, it forces the UA device designers to size the ultrasonic system at a frequency of practically at least >35 kHz, if the powder is to be utilised in additive manufacturing. The atomisation temperature (i.e., at the surface of the molten metal pool) has a secondary effect, and, as explained above, preferably should be high enough to decrease the surface tension but low enough to prevent evaporation of individual elements. Although, when needed, occasional overheating can also give the required results – a

finer powder at a higher production output. This is similar to the case of a lowered viscosity in the pool – see Figure 5, presenting the atomisation chamber cross-section (perpendicular to the view shown in Fig. 1), where the red/orange zones show high temperature areas directly around the electric arc.

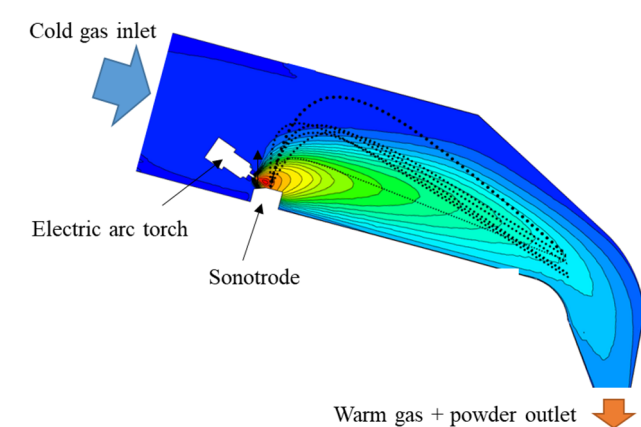


Fig. 5. The temperature profile of the gas and droplet trajectories during the atomisation

Note that the proportion of surface tension to density of titanium and its alloys is larger than of steel or Ni- / Co-based alloys, so the Ti powders are coarser than those based on Fe / Ni / Co. This fact should be known for any physics-based atomisation techniques and, among others, it is the reason why the Ti-based powders are much more expensive than other common alloys, especially if they are produced by, e.g., gas atomisation, where only a small part of the output yields fractions $<63 \mu\text{m}$. For example, for ultrasonic atomisation at 35 kHz, as tested on the ATO system with a set atomisation temperature of $\sim 3000 \text{ deg K}$, the UA system would yield $D_{32} \sim 47 \mu\text{m}$ for AISI 316L steel powder, $\sim 52 \mu\text{m}$ for Inconel 718 (Ni-based), while $62 \mu\text{m}$ for Ti6Al4V. Similar results are presented in [12], where a test with laser beam heating for a frequency of 40 kHz produced AISI 316L powder with average diameters within the range of $49\text{--}66 \mu\text{m}$ – dependent on the atomisation intensity (i.e., vibration amplitude), which underlines the value of more accurate modelling of the process with formulas (1-2) instead of a simplified one (3), where estimation errors can be as high as $+10\% / -20\%$ on D_{32} (i.e., usually finer particles are produced than those expected from the formula (3)).

The key feature of the ATO system is a cooled sonotrode. Its patent-protected design considers factors such as thermal fatigue at its hot end, the need to stabilise its temperature by liquid cooling of the non-working surfaces, the heat balance

of the melting sub-system to stabilise the temperature in the pool at the optimal level, low damping of ultrasonic vibrations, risk of high cycle fatigue. The report of the OEM [31] discusses the main design challenges for the ATO system.

The power rating of the ultrasonic system to perform ejection and transport actions on the stream of droplets is sized to ensure at the same time:

- demand for the surface tension and viscosity to separate droplets from the pool,
- initial kinetic energy of droplets to allow their transportation, i.e., droplets should obtain proper momentum at the start.

The latter should be high enough in order to assure high utilisation of the raw material, because droplets cannot hit any inner surface of the atomisation chamber as these particles would be lost from the powder production. So, the power rating of the sub-system depends on the required droplet size (frequency and temperature related), density, surface tension, and viscosity (both temperature related). In practice, at a lower atomisation temperature (close to the liquidus), the demand for the ultrasonic power increases as larger droplets are formed and there is a higher surface tension and viscosity to overcome. An example of particle statistical distribution (PSD) is presented in Figure 3. The chart compares the cumulative distributions of the powder before classification for gas (EIGA in this example) and ultrasonic atomisation methods (at the standard setup to maximise the output). A significant disadvantage of gas atomisation is, as documented by ALD (2016) (black triangles on the chart) and Kirchner et al. (2016) (black dots), that its median particles have a size of $70\text{--}90 \mu\text{m}$, while fewer than 30% of the Ti6Al4V have a size of $<63 \mu\text{m}$ desirable for AM. Similar findings were presented in [20] for TiAl powder (blue dots on the chart) with 32% of the batch $<63 \mu\text{m}$. Similar values ($D_{50} = 51.2$, $D_{90} = 117.8 \mu\text{m}$) were reported in [32] for the Ti45Al2Nb2Mn powder from the EIGA process. Contrary to the GA, the ultrasonic atomisation at a frequency of 35 kHz can yield a powder with a median of $62 \mu\text{m}$, while more than half of the batch meets the AM requirements. As the powder is finer by default at a higher ultrasonic frequency, it can be expected that at, e.g. 52 kHz $\sim 95\%$ of the batch will be under $63 \mu\text{m}$. The PSD was also analysed for the Ti25Al12Nb alloy (blue lines and points) – the produced powder can be finer in similar atomisation conditions, e.g., its median is at $52 \mu\text{m}$. As shown in the graph, the main advantage of the UA method over the GA methods is that it can produce the majority of a batch with a powder size close to the value expected by the additive manufacturing market. Although

the UA output (mass rate) is less than the GA, the ATO system is still capable of producing the required powder in a single run with a high conversion rate (>95% of the raw material converted into unclassified powder). As a result, the operating cost of the ATO system is much lower than in the case of the GA, PREP or PA methods, since it eliminates remelting and repeated atomisation of the overly coarse powder.

2.3. The function of gas in the process

The ultrasonic atomisation of molten metals can take place in the presence of gas or in a vacuum due to the fact that, in general terms, the UA process is pressure independent and can be carried out in gas at any pressure (but reasonably much lower than for GA). The tested UA unit of the ATO system operated at 1.1 bar, i.e., slightly above the ambient pressure to simplify the design of the chamber and downstream equipment (e.g., system sealing, gas-powder separation, cooling, EHS issues). Most importantly, it allows running the process at a low inert gas consumption, while the cost of the process gas can take ~10% of the total operating cost only. In comparison, the gas atomisation operates at a considerably higher process gas cost because of the much higher pressure (15-60 bar).

In the case of low-density alloys like Ti-based, the challenge is that the ejected droplets have low kinetic energy therefore gas turbulence can deflect the trajectories of the droplets. As a result, they can stay in the stagnation zone and then stick to the chamber wall, instead of traveling towards the outlet and the gas-powder separation unit. Consequently, simulations were carried out to improve the gas's velocity profile inside the chamber to enhance the yield of powder from the feedstock. Thus, stagnation zones, which occur when the droplets' course is not adequately controlled, were eliminated. The sonotrode ejects them in a stochastic manner, with some variation in direction and diameter – see marked powder trajectories by dotted lines in Figure 5. Optimally, aerodynamic drag should be controlled, as different kinetic energies of the droplets can cause collisions with each other, which decreases the sphericity of the powder. A CFD simulation (on the Fluent software, example in Fig. 5.) was a proper tool to visualise the lines of gas flow incl. thermal effects around concentrated heat sources (electric arc) and to determine the stagnation and turbulence zones, which affect the droplets' trajectory and cooling rate. The design of features deflecting the gas flow, and the gas profile downstream from the sonotrode were improved. As a result, it was possible to recover >98% of useful powder from the feedstock.

3. Example of titanium alloy atomisation

The UA system, as described above was tested on a production scale during atomisation of the titanium alloy Ti6Al4V as per AMS 4928, UNS R56200 and ASTM B265 standards – known on the market also as Titanium Grade 5 or Ti64. This material is the most commonly used titanium alloy today. It is classified as the ($\alpha+\beta$)-alloy by its microstructure. It accounts for 50 % of the whole production of titanium alloys, because of its very well-balanced properties, such as low density, ductility, good resistance to corrosion and oxidation. It is used at high operating temperatures where mechanical properties play a key role, for example, in gas turbines, aeroplanes, jet engines and biomedical applications [33].

The challenges in converting this and other Ti-based alloys into powder include:

- Relatively high melting temperature – liquidus at 1660°C;
- High surface tension, which means that any atomisation method needs to be more vigorous to form fine powder with the required PSD;
- Strict requirements for chemical composition (no contaminants, an equal amount of alloying elements) because one expects to keep the composition as similar as possible during the conversion from raw material to powder;
- Limited content of oxygen – no more than 0.2%, preferably <0.13% as in the ELI specification.

The alloy Ti6Al4V has the physical properties as shown in Table 1 and Figure 6; the reference values are based on the average values from the tests reported in [34,35,28]. The raw material for tests was supplied in the form of a 1.5 mm wire.

Table 1.
Properties of the Ti6Al4V alloy

Property	Value
Density @ 20 deg	4430 kg/m ³
Density @ MP	4055 kg/m ³
Surface tension @ MP	1.55 N/m
Solidus	1604°C = 1879 K
Liquidus	1660°C = 1933 K

The tests were carried out at an ultrasonic frequency of 35 kHz and at a moderate heating rate to keep the molten metal close to the optimal temperature of 1.3-1.5 times liquidus (absolute) in order to obtain a fine powder of premium quality at a high production output. The atomisation chamber was pressurised and ventilated with

pure argon, and the electric arc between the non-consumable electrode and the sonotrode was set at 130 amps in pure argon. The argon at both inlets was supplied at a temperature of 20°C.

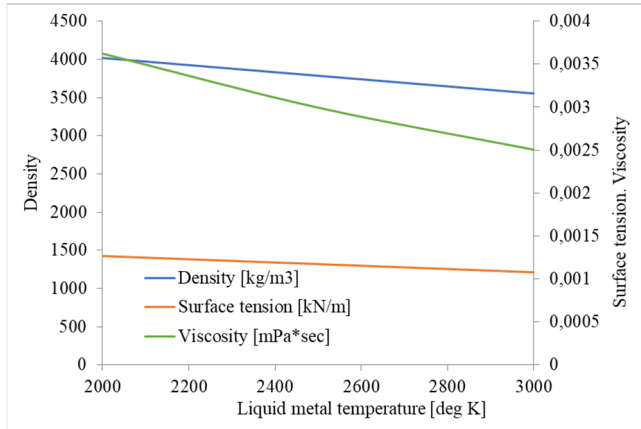


Fig. 6. The properties of the molten Ti6Al4V alloy as a function of temperature

4. Description of the achieved properties for the Ti6Al4V powder

4.1. Statistical distribution of powder diameters

The particle size distribution (PSD) of two Ti6Al4V powder batches was checked on the KEYENCE VHX-6000 microscope and post-processed by binary image processing. The powder was then classified according to DIN 66165-1 with a sieve shaker brand Multiserw model LPzE-3e at a frequency of 50 Hz. The compared batches were produced by:

1. Metco Oerlicon Metco as a commercially available powder for additive manufacturing, specification MetcoAdd Ti64 G23-A classified to $45 +15 \mu\text{m}$;
2. 3D Lab Ltd. on their ATO system at the ultrasonic frequency of 35 kHz and then classified to the range: $63 +20 \mu\text{m}$.

The obtained results are:

- Overall 94% of the raw material (wire) was converted into powder $<100 \mu\text{m}$ (i.e., a particle size useful for AM, sintering, and coatings), hence the scrap rate was much lower than in the GA process because, in this case, the conversion rate $<100 \mu\text{m}$ typically yields 60-85% as documented in [16] for the lower value and in [19] for the higher value,
- Then 70.3% of the powder mass was classified in the range of $63 +20 \mu\text{m}$, i.e., applicable for the AM market,

which is also a much better value than for the GA process (typically $\sim 30\%$, see Fig. 3),

- Eventually, the key powder batch classified in the range of $63 \pm 20 \mu\text{m}$ are $D_{10} = 40.2$, $D_{50} = 52.0$, $D_{90} = 60.8 \mu\text{m}$, if based on the particle counting and $D_{10} = 45.4$, $D_{50} = 55.0$, $D_{90} = 62.4 \mu\text{m}$, if based on the volume percentile.

The chart with PSD is shown in Figure 7. The measured values of MetcoAdd powder were not exactly as stated by the OEM [36], although the measurement method was different. The producer describes their methods as “for the nominal range, particle size $45 \mu\text{m}$ or the above measured by sieve (ASTM B214), below $45 \mu\text{m}$ by laser diffraction (ASTM C 1070, Microtrac). Fractional analysis (D_{90} , D_{50} , D_{10}) are nominal values by laser diffraction”, and the producer informs, that $D_{10} = 18$, $D_{50} = 32$, $D_{90} = 50 \mu\text{m}$. The PSD, as measured in the test campaign, is based on the optical method and a particle count, and the powder has parameters $D_{10} = 16.1$, $D_{50} = 31.0$, and $D_{90} = 53.4 \mu\text{m}$. Accordingly, if based on the volume percentile, the same powder has parameters $D_{10} = 29.0$, $D_{50} = 47.3$, $D_{90} = 77.8 \mu\text{m}$.

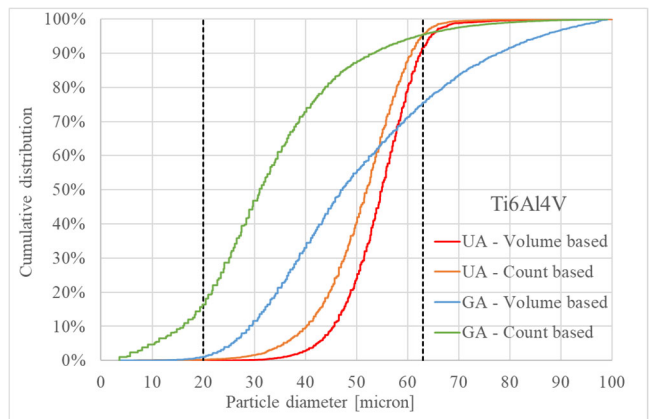


Fig. 7. Cumulative statistical distribution for Ti6Al4V powder batches from gas (GA) and ultrasonic (UA) atomisation after classification

Considering an industrial application of the powder, such as sintering, the PSD of powders should be compared based on their volume percentiles, because this parameter, as mass-related, is the most representative. So, one can see that a UA powder made at 35 kHz and the classified $63 \pm 20 \mu\text{m}$ have $D_{50}(\text{Vol.}\%) = 55.0 \mu\text{m}$ vs $47.3 \mu\text{m}$ for GA, i.e., only 16% more, which would have a minor impact on the properties of the sintered product. If requested, to reach exactly the same $D_{50}(\text{Vol}\%) \sim 47 \mu\text{m}$ for both powder batches, the UA powder should be further classified to range $50 +20 \mu\text{m}$. Nevertheless, the final sintered product would have a much

lower roughness if it is made of UA powder like this, because of the much lower content of large particles.

The auxiliary quality metrics of powder are used, and they are usually Span (the lower the better) and Sphericity (the higher the better). Both parameters are correlated to the flowability of the powder and, therefore, improve the uniformity of the powder distribution in the sintering bed. These parameters can be defined as:

$$\text{Span} = (D_{90} - D_{10}) / D_{50} \quad (4)$$

$$\text{Sphericity} = D_{\min} / D_{\max} \quad (5)$$

Note that this definition of sphericity is based on the ratio of the minimum to maximum particle diameters and can be interpreted as the opposite of its Anisotropy = 1 – Sphericity, reported in some research reports and proven by experiments. In general, the UA powder has better quality metrics, i.e., lower span / narrower statistical distribution and higher sphericity / lower anisotropy.

Overall powder metrics for GA, PA and UA powders are similar, if directly compared. Check the Table 2 with all PSD metrics count-based for commercially available GA / PA powders. The MetcoAdd Ti64 G23 [36] includes the material specification for GA powder. The PA powder data

from AP&C is available from [37,38]. The PA powder data from PyroGenesis is available from [39,40]. Note that D10/D50/D90 values in Table 2 are as declared by the powder producers and are based on the particle count and a slightly different testing method (laser diffraction) than the one used by the authors (optical microscope). The practical differences in both methods have been recently discussed in [41]. Table 3 compares GA and UA powders based on their PSD expressed as the volume percentiles, because it is more representative of batch qualification.

Additionally, a much narrower distribution (i.e., of lower Span) and a better Sphericity of the UA powder – as reported in Table 2, can also be observed in Figure 8. The left side of Figure 8 exemplifies the MetcoAdd™ Ti64 G23 powder made by Metco Oerlicon in the EIGA process, the right side shows the particles produced in the UA process in the ATO system. One can expect that a balanced grain size distribution positively influences the maximum packing density and, therefore, the density of the generated component. The flowability also depends on the grain size distribution. This is validated in the next section. Fig. 8 also proves that particularly large or small particles are not included in the UA batch.

Table 2.

Particle size distribution (count based) of the Ti-6Al-4V powders as declared by their supplier

EIGA	PA	PA	UA	UA	UA
Brand	Oerlicon MetcoAdd	AP&C	PyroGenesis	3D Lab – ATO	3D Lab – ATO
Sieve classification	-45 +15	- 63 + 20	- 52 +20	None	-63 + 20
D10, μm	18	24	25.9	41.2	40.2
D50, μm	32	44	36.7	51.4	51.4
D90, μm	50	61	50.3	63.4	60.8
Span	0.81	0.77	0.66	0.43	0.37
Average Sphericity	0.76	0.82	0.88	0.88	0.90

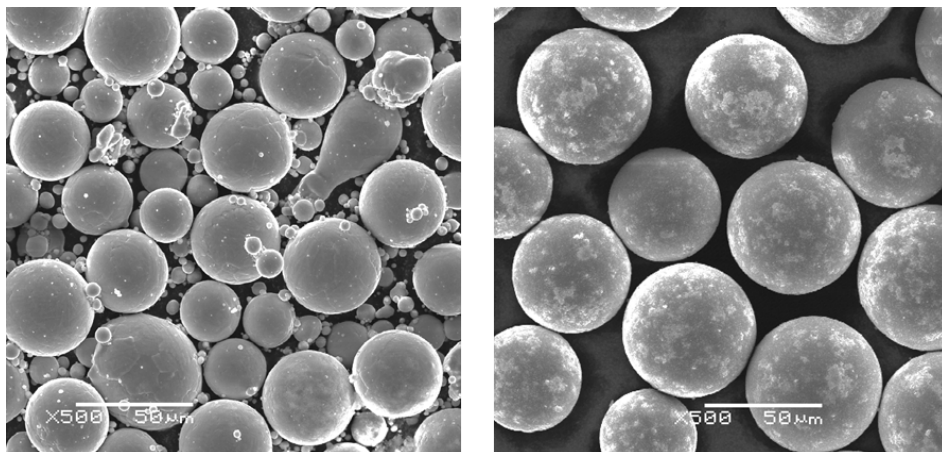


Fig. 8. Examples of SEM pictures of the GA (left) and the UA (right) powder

Table 3.

Particle size distribution (volume % based) of the Ti-6Al-4V powders as measured in the test campaign

Production method	EIGA	UA	UA
Brand	Oerlicon MetcoAd	3D Lab – ATO	3D Lab – ATO
Sieve classification	-45 +15	None	-63 + 20
D10, μm	29	47.1	45.4
D50, μm	47.3	58.6	55.0
D90, μm	77.8	79.8	62.4
SMD, μm	37.19	N/A	52.54

4.2. Physical properties of powders

Usually, the main properties of powders applied in additive manufacturing are tap, apparent and true densities, flowability, and porosity related to gas bubbles. A summary of these properties of the UA vs. GA and PA powders is provided in Table 4. The values for the EOS powders come from [40,42,43]. The properties of AP&C powder are available from the datasheet [38]. The additional metrics in Table 4 are:

- Hausner ratio defined as the ratio between tap and apparent densities (the lower, the better, as better flowability and probably lower porosity after sintering are expected),
- powder porosity defined as the number of voids (gas bubbles) based on the proportion of true and theoretical density for the Ti6Al4A (4430 kg/m^3),
- Sauter mean diameter (SMD) defined as the diameter of an ideal sphere that has the same volume/surface area ratio as the average particle from the batch tested. Because the laser beam heat during AM melting is largely carried through the particle outer surfaces, and the enthalpy required for melting is linked to the particle mass/volume, this parameter is of practical importance in the AM application. As a result, a finer powder has a greater area-to-volume ratio and can be heated more

easily with a laser beam (i.e., higher efficiency of thermal conversion can be anticipated). The SMD value here is based on PSD calculations. It covers the min-max diameter range for particles that are not completely spherical (i.e., the volume/area ratio is obtained for a sum of all ellipsoids in PSD).

The batches of UA and GA (MetcoAdd from EIGA process) powders were tested with the following methods:

- True density – an AccuPyc II 1340 gas displacement pycnometry system was used to measure according to the ASTM B923 standard,
- Apparent and tap densities – measured according to the ASTM B212,
- Flowability – flow rate tested by means of a calibrated funnel on the Hall flowmeter per the ISO4490:2018 standard.

The comparison of UA, GA and PA powders confirmed that the UA powder has a better flowability (25.1-27.9 sec/50 gr) and a higher density for all its three types. The higher true powder density and, in other words, the negligible porosity of the UA powder can be attributed to a lower propensity for collecting gas bubbles during droplet formation. The research in [44] estimated that the titanium powder produced by the EIGA method has a porosity at a level of 1.5% for the particles classified $<75 \mu\text{m}$. Also, higher levels of porosity 1.88% for the PA powder (Ti5Al4V from PyroGenesis) were reported in [40]. The measurements taken on the UA powder show that its porosity is lower (0.27%) than that of the commercially available EIGA powder (1.04%) – see Table 4. Such a higher content of gas bubbles is not surprising as the UA is produced in the ATO system at low pressure (~ 1 bar), while GA powders are made by the brute force of the high-pressure gas action (15-60 bar), as deliberated in [45].

The GA powder is characterised by a Sauter mean diameter (SMD) value of 37.19 microns, whereas the UA powder has a value of 52.54 microns. For the same mass of the batches, this indicates that the GA batch has 29% more

Table 4.

Physical properties of the Ti-6Al-4V powders in application to additive manufacturing

Production method	EIGA	EIGA	PA	UA
Brand	MetcoAdd™ Ti-6Al-4V ELI	EOS	AP&C	3D Lab ATO
Sieve classification	-63+20	-50+20	-63+20	-63+20
Tap density, gr/cm^3	N/A	2.55 – 2.83	>2.70	2.86
Apparent density, gr/cm^3	N/A	2.36 - 2.46	>2.40	2.62
True density, gr/cm^3	4.38	N/A	N/A	4.42
Hausner ratio	N/A	1.11	1.12	1.09
Powder porosity	1.04%	-	-	0.27%
Flow rate, sec/50 gr	40.8	35.0 - 39.2	< 35	25.1 - 27.9

surface area than the UA batch. On the one hand, such a difference could be somewhat of a disadvantage during the laser beam melting, but on the other hand, the lower area of the UA powder reduces its propensity for oxidising as less oxygen can be bonded on the overall smaller surface of the particles (e.g., during contamination in the production and storage) and this effect can be observed in the results of the chemical composition of the powders.

4.3. Chemical composition

The chemical composition of the raw material in the form of a wire (per titanium grade 5 specification) and the powder produced from it was determined by inductively coupled plasma-optical emission spectrometry (ICP-OES method). The variations in the composition were small – see Table 5 – and the powder meets the ASTM B265 Grade 5 specification criteria. More specifically, minor reductions of the aluminium content were observed from 6.6% to 6.0%. This situation resulted from a trade-off between better quality and higher production rate, due to the fact that the production batch was atomised at a relatively high temperature – the analytical model of heat balance estimated it at ~3000 K in the gas directly above the pool. The processed material stayed in a liquid state for a few seconds, so minor evaporation of Al was observed, but due to the short time involved, the deviation in the powder composition was negligible. Another important element for titanium alloys is the amount of oxygen – here, the value was very low, 0.0039% and only slightly higher than in the raw material, 0.0036%. The atomisation process in the argon pressurised chamber can produce practically an oxygen-free powder, while typically, the PA / GA powders of the competitors keep the oxygen content in the range 0.11%-0.19% – as based on screening in [19,40].

Table 5. Chemical composition (wt. %) of the raw material (wire) vs UA powder for titanium grade 5

Element	Specification ASTM B265	Wire	UA powder
Ti	balance	balance	balance
Al	5.50 – 6.75	6.6	6.0
V	3.50 – 4.50	4.0	4.0
Fe	<0.4	0.21	0.28
C	<0.08	0.022	0.025
N	<0.05	<0.005	<0.005
H	<0.015	0.0053	0.0047
O	< 0.20	0.0036	0.0039
Cu	<0.1%	< 0.01	0.036

Surely the chemical composition of the powder is suitable for further SLM printing. Actually,, the powder could even meet the criteria of the specification for Ti6Al4V Grade 23 and ELI with an oxygen limit of 0.13% if the raw material had a reduced amount of iron (limit <0.25% for ELI).

4.4. Particle morphology

The particle shape was determined by the (SEM) according to DIN EN ISO 3252. The particles presented in Figure 8 show a spherical shape of the UA powder from the ATO system (right picture), which is required by the AM market and indicates the good flowability and high packing density of the powder. Furthermore, the SEM-picture of UA does not show agglomerates and satellite particles, which are common for gas atomisation (picture on the right).

The properties of the Ti6Al4V alloy depend on the microstructure, the size and arrangement of the α - and β -phase. The α/β proportion depends on the cooling process. Fast quenching (like during atomisation with a rate of > 500 K/sec) leads to the martensitic transformation of the β -phase with a fine structure. Both forms of microstructures can exist in fine and coarse distribution, although almost 100% martensite α' is typical for fine powders. The XRD scan (Fig. 9) of the powder surface shows that the Bragg peaks belong 100% to the α' phase for the UA powder from the ATO system and the referenced EIGA powder (brand MetcoAdd™). The XRD scans have not revealed other phases in both powders.

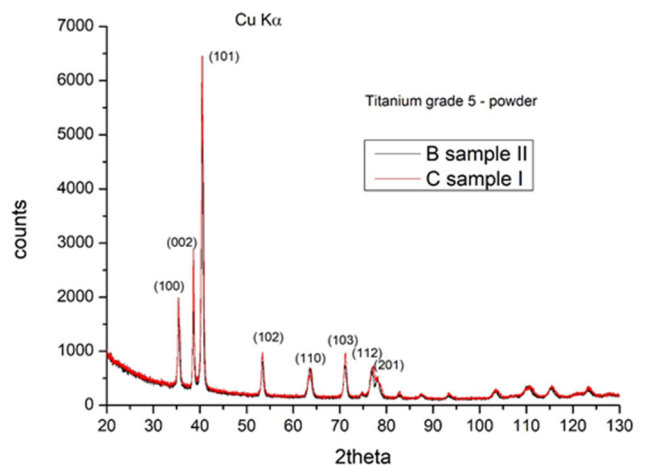


Fig. 9. XRD scan of the Ti6Al4V powder – sample B for the EIGA powder, C for the UA powder produced on the ATO system

5. Conclusions

The quality and performance of the Ti alloy and components are, of course, highly dependent on the powders utilised. The chemical composition and physical qualities for the AM application are the most stringent: high purity, high sphericity and flowability, no trapped gas-bubble porosity, and a low oxygen content. In general, a powder with a high flowability has, by default, a highly spherical form and a limited amount of very fine particles. Furthermore, preferably the powders should have a high apparent density and tap density, which have an advantageous impact on the low porosity and homogeneity of the sintered components. All these parameters were examined in the paper on the Ti6Al4V powder produced by a novel ultrasonic atomisation method (UA) on the ATO system.

The unique and patent protected feature of the ATO system is that it integrates the raw material melting by an electric arc with the atomisation from the molten metal pool. The powder is produced at a low pressure, so the inert gas consumption and atomisation chamber is much lower and simpler than that of the gas atomisation method (GA). The presented results reveal that the UA powder can have a premium quality in terms of:

- High production yield as 94% of the raw material is converted to a useful powder with particles <100 µm,
- Almost all particles are very spherical, with the negligible share of satellites or particles with voids or deformed parts,
- High tap, apparent and true density,
- Very good flowability,
- Stable chemical composition (low variation compared to raw material composition),
- Similar particle morphology to the GA standard powders for the AM market.

Moreover, the ultrasonic atomisation method can be a cost competitive option compared with gas atomisation. This is because of the much higher yield of useful fine powder from a production batch and low consumption of pure argon since the atomisation takes place in a small chamber at an ambient pressure.

Funding sources

Production of the powder batches was supported by the 3D Lab Ltd from its internal R&D program. The assessment of the powder properties was supported by Koszalin University of Technology.

References

- [1] Z.Z. Fang, J.D. Paramore, P. Sun, K.S. Ravi Chandran, Y. Zhang, Y. Xia, F. Cao, M. Koopman, M. Free, Powder metallurgy of titanium – past, present, and future, *International Materials Reviews* 63/7 (2018) 407-459. DOI: <https://doi.org/10.1080/09506608.2017.1366003>
- [2] L.A. Dobrzański, L.B. Dobrzański, A.D. Dobrzańska-Danikiewicz, M. Kraszewska, Manufacturing powders of metals, their alloys and ceramics and the importance of conventional and additive technologies for products manufacturing in Industry 4.0 stage, *Archives of Materials Science and Engineering* 102/1 (2020) 13-41. DOI: <https://doi.org/10.5604/01.3001.0014.1452>
- [3] D. Chasoglou, Powder Manufacturing and Characterization, lecture by Hogan AB for European Powder Metallurgy Association Summer School, 2016. Available from: <https://www.epma.com/document-archive/summer-school-presentations/summer-school-2016/604-powder-manufacturing-characterization/file>
- [4] P. Sun, Z.Z. Fang, Y. Zhang, Y. Xia, Review of the Methods for Production of Spherical Ti and Ti Alloy Powder, *JOM* 69/10 (2017) 1853-1860. DOI: <https://doi.org/10.1007/s11837-017-2513-5>
- [5] S. Tamas-Williams, P.J. Withers, I. Todd, P.B. Prangnell, The Influence of Porosity on Fatigue Crack Initiation in Additively Manufactured Titanium Components, *Scientific Reports* 7 (2017) 7308. DOI: <https://doi.org/10.1038/s41598-017-06504-5>
- [6] D. Zhang, W. Wang, Y. Guo, S. Hu, D. Dong, R. Poprawe, J.H. Schleifenbaum, S. Ziegler, Numerical simulation in the absorption behavior of Ti6Al4V powder materials to laser energy during SLM, *Journal of Materials Processing Technology* 268 (2019) 25-36. DOI: <https://doi.org/10.1016/j.jmatprotec.2019.01.002>
- [7] M. Bielecki, J. Kluczyński, Ł. Słoboda, K. Grzelak, Manufacturing of metallic powders for am market by ultrasonic atomisation method, *Proceedings of Metal Additive Manufacturing Conference “MAMC 2021”*, Vienna, Austria, 2021.
- [8] M. Bielecki, R. Rałowicz, Ł. Słoboda, Method and device for producing heavy metal powders by ultrasonic atomisation, *International Patent Submission WO2021009683*, 2020.
- [9] R. Rałowicz, L. Zrodowski, J. Rozpendowski, K. Kaczynski, W. Laczisz, M. Ostrysz, Device for the manufacturing of spherical metal powders by an ultrasonic atomisation method, *International Patent Submission WO2019092641*, 2018.

- [10] K. Kaczyński, R. Rałowicz, M. Bielecki, A method for evacuation of powder produced by ultrasonic atomisation and a device for implementing this method, International Patent Submission WO2021009708A1, 2020.
- [11] S. Komarov, M. Kuwabara, O.V. Abramov, High Power Ultrasonics in Pyrometallurgy: Current Status and Recent Development, *ISIJ International* 45/12 (2005) 1765-1782.
DOI: <https://doi.org/10.2355/isijinternational.45.1765>
- [12] S. Habib Alavi, S.P. Harimkar, Effect of vibration frequency and displacement on melt expulsion characteristics and geometric parameters for ultrasonic vibration-assisted laser drilling of steel, *Ultrasonics* 94 (2019) 305-313.
DOI: <https://doi.org/10.1016/j.ultras.2018.08.012>
- [13] Ł. Żrodowski, R. Wróblewski, T. Choma, B. Moronczyk, M. Ostrysz, M. Leonowicz, W. Łacisz, P. Błyskun, J.S. Wróbel, G. Cieślak, B. Wysocki, C. Żrodowski, K. Pomian, Novel Cold Crucible Ultrasonic Atomization Powder Production Method for 3D Printing, *Materials* 14/10 (2021) 2541. DOI: <https://doi.org/10.3390/ma14102541>
- [14] S. Biswas, S. Habib Alavi, B. Sedai, F.D. Blum, S.P. Harimkar, Effect of ultrasonic vibration-assisted laser surface melting and texturing of Ti-6Al-4V ELI alloy on surface properties, *Journal of Materials Science and Technology* 35/2 (2019) 295-302.
DOI: <https://doi.org/10.1016/j.jmst.2018.09.057>
- [15] 3D Lab Ltd., Ato Lab+ product review - small scale atomizer for reactive metal materials, 2019. Available from: <https://www.youtube.com/watch?v=Zr-4FV29za0>
- [16] Repowder, Project Repository, 2021. Available from: <https://repowder.dtu.dk/>
- [17] R. Pohlman, K. Heisler, M. Cichos, Powdering aluminum and aluminum alloys by ultrasound, *Ultrasonics* 12/1 (1974) 11-15.
DOI: [https://doi.org/10.1016/0041-624X\(74\)90080-8](https://doi.org/10.1016/0041-624X(74)90080-8)
- [18] ALD Vacuum Technologies GmbH, Metal Additive Manufacturing - EIGA and VIGA: Metal Powder Inert Gas Atomization Equipment, 2016.
Available from: https://www.ald-vt.com/wp-content/uploads/2018/01/Metal_Additive_Manufacturing.pdf
- [19] A. Kirchner, B. Klöden, T. Weißgärber, B. Kieback, Powders for Additive Manufacturing, Proceedings of the World PM2016 – AM – Powder Characteristics Congress and Exhibition, Hamburg, Germany, 2016.
- [20] V. Güther, Manufacturing of TiAl Powders based on Electrode Induction Gas Atomization, Proceedings of the Titanium Europe Conference, Vienna, Austria, 2019.
- [21] R.J. Lang, Ultrasonic atomization of liquids, *The Journal of the Acoustical Society of America* 34 (1962) 6-9. DOI: <https://doi.org/10.1121/1.1909020>
- [22] B. Avvaru, M.N. Patil, P.R. Gogate, A.B. Pandit, Ultrasonic atomisation: effect of liquid phase properties, *Ultrasonics* 44/2 (2006) 146-158. DOI: <https://doi.org/10.1016/j.ultras.2005.09.003>
- [23] K.A. Ramisetty, A.B. Pandit, P.R. Gogate, Investigations into ultrasound induced atomisation, *Ultrasonics Sonochemistry* 20/1 (2013) 254-264. DOI: <https://doi.org/10.1016/j.ultsonch.2012.05.001>
- [24] M. Dobre, L. Bolle, Visualisation and Analysis of Liquid Film Surface Patterns Formed on Ultrasonic Atomizers, Proceedings of the ILASS-Europe'99, Toulouse, France, 1999.
- [25] A. Sugondo, Sutrisno, W. Anggono, O. Anne, Effect of Frequency on Droplet Characteristics in Ultrasonic Atomization Process, *E3S Web of Conferences* 130 (2019) 01002.
DOI: <https://doi.org/10.1051/e3sconf/201913001002>
- [26] A.J. Yule, Y. Al-Suleimani, On droplet formation from capillary waves on a vibrating surface, Proceedings of the Royal Society A 456 (2000) 1069-1085. DOI: <https://doi.org/10.1098/rspa.2000.0551>
- [27] Y. Al-Suleimani, A.J. Yule, A.P. Collins, How Orderly is Ultrasonic Atomisation?, Proceedings of the ILASS-Europe'99, Toulouse, France, 1999.
- [28] K. Zhou, H.P. Wang, J. Chang, B. Wei, Experimental study of surface tension, specific heat and thermal diffusivity of liquid and solid titanium, *Chemical Physics Letters* 639 (2015) 105-108.
DOI: <https://doi.org/10.1016/j.cplett.2015.09.014>
- [29] R.K. Wunderlich, Surface Tension and Viscosity of Industrial Ti-Alloys measured by the Oscillating Drop Method on Board Parabolic Flights, *High Temperature Materials and Processes* 27/6 (2008) 401-412. DOI: <https://doi.org/10.1515/HTMP.2008.27.6.401>
- [30] J.R. Raush, Thermophysical and Thermochemical Property Measurement and Prediction of Liquid Metal Titanium Alloys with Applications in Additive Manufacturing, PhD Thesis, Louisiana State University, Baton Rouge, 2016.
- [31] M. Bielecki, How Ansys helped to make powder for additive manufacturing?, 2020. Available from: <https://mesco.com.pl/blog/238-blog-mes/1180-how-ansys-helped-to-make-powder-for-additive-manufacturing>
- [32] R. Muñoz-Moreno, E.M. Ruiz-Navas, B. Srinivasarao, J.M. Torralba, Microstructural Development and

- Mechanical Properties of PM Ti-45Al-2Nb-2Mn-0.8 vol.%TiB₂ Processed by Field Assisted Hot Pressing, *Journal of Materials Science and Technology* 30/11 (2014) 1145-1154.
DOI: <https://doi.org/10.1016/j.jmst.2014.08.008>
- [33] J. Klimas, A. Łukaszewicz, M. Szota, K. Laskowski, Work on the modification of the structure and properties of Ti6Al4V titanium alloy for biomedical applications, *Archives of Materials Science and Engineering* 78/1 (2016) 10-16. DOI: <https://doi.org/10.5604/18972764.1226308>
- [34] Z. Liu, C. Huang, C. Gao, R. Liu, J. Chen, Z. Xiao, Characterisation of Ti6Al4V powders produced by different methods for selective electron beam melting, *Journal of Mining and Metallurgy B: Metallurgy* 55/1 (2019) 121-128.
DOI: <https://doi.org/10.2298/JMMB181025008L>
- [35] M. Mohr, R. Wunderlich, R. Novakovic, E. Ricci, H.-J. Fecht, Precise Measurements of Thermophysical Properties of Liquid Ti-6Al-4V (Ti64) Alloy On Board the International Space Station, *Advanced Engineering Materials* 22/7 (2020) 2000169. DOI: <https://doi.org/10.1002/adem.202000169>
- [36] Specification MetcoAdd Ti64 G23, 2021.
Available from: https://www.oerlikon.com/ecomaXL/files/metco/oerlikon_OAM_Ti-6Al-4V_G_5_23_1910.pdf
- [37] T. Thiede, T. Mishurova, S. Evsevlev, I. Serrano-Munoz, C. Gollwitzer, G. Bruno, 3D Shape Analysis of Powder for Laser Beam Melting by Synchrotron X-ray CT, *Quantum Beam Science* 3/1 (2019) 3. DOI: <https://doi.org/10.3390/qubs3010003>
- [38] Powder specification AP&C Ti-6Al-4V, 2021.
Available from: <https://www.advancedpowders.com/powders/titanium/ti-6al-4v-5>
- [39] Powder specification Pyrogenesis Ti-6Al-4V, 2021.
Available from: <https://www.pyrogenesis.com/wp-content/uploads/2019/10/PyroGenesis-Additive-PRODUCT-SPEC-SHEET-Ti64-Grade-23-ELI-15-45-microns-1.pdf>
- [40] S.E. Brika, M. Letenneur, C.A. Dion, V. Brailovski, Influence of particle morphology and size distribution on the powder flowability and laser powder bed fusion manufacturability of Ti-6Al-4V alloy, *Additive Manufacturing* 31 (2020) 100929.
DOI: <https://doi.org/10.1016/j.addma.2019.100929>
- [41] J. Grubbs, K. Tsaknopoulos, C. Massar, B. Young, A. O'Connell, C. Walde, A. Birt, M. Siopis, D. Cote, Comparison of laser diffraction and image analysis techniques for particle size-shape characterization in additive manufacturing applications, *Powder Technology* 391 (2021) 20-33.
DOI: <https://doi.org/10.1016/j.powtec.2021.06.003>
- [42] H. Gu, H. Gong, J.J.S. Dilip, D. Pal, A. Hicks, H. Doak, B.E. Stucker, Effects of Powder Variation on the Microstructure and Tensile Strength of Ti6Al4V Parts Fabricated by Selective Laser Melting, *International Journal of Powder Metallurgy* 51 (2015) 35-42.
- [43] B. Fotovvati, E. Asadi, Size effects on geometrical accuracy for additive manufacturing of Ti-6Al-4V ELI parts, *The International Journal of Advanced Manufacturing Technology* 104 (2019) 2951-2959.
DOI: <https://doi.org/10.1007/s00170-019-04184-1>
- [44] R.-P. Guo, L. Xu, B.Y.-P. Zong, R. Yang, Characterization of Prealloyed Ti-6Al-4V Powders from EIGA and PREP Process and Mechanical Properties of HIPed Powder Compacts, *Acta Metallurgica Sinica (English Letters)* 30/8 (2017) 735-744. DOI: <https://doi.org/10.1007/s40195-017-0540-4>
- [45] M. Iebba, A. Astarita, D. Mistretta, I. Colonna, M. Liberini, F. Scherillo, C. Pirozzi, R. Borrelli, S. Franchitti, A. Squillace, Influence of Powder Characteristics on Formation of Porosity in Additive Manufacturing of Ti-6Al-4V Components, *Journal of Materials Engineering and Performance* 26 (2017) 4138-4147. DOI: <https://doi.org/10.1007/s11665-017-2796-2>



© 2023 by the authors. Licensee International OCSCO World Press, Gliwice, Poland. This paper is an open-access paper distributed under the terms and conditions of the Creative Commons Attribution-NonCommercial-NoDerivatives 4.0 International (CC BY-NC-ND 4.0) license (<https://creativecommons.org/licenses/by-nc-nd/4.0/deed.en>).